JPE 16-6-23

http://dx.doi.org/10.6113/JPE.2016.16.6.2221
ISSN(Print): 1598-2092 / ISSN(Online): 2093-4718

A Novel Three-Phase Four-Wire Grid-Connected Synchronverter that Mimics Synchronous Generators

Qian Tan†, Zhipeng Lv**, Bei Xu***, Wenqian Jiang****, Xin Ai*, and Qingchang Zhong**

†,*State Key Laboratory of Alternate Electrical Power System with Renewable Energy Sources, North China Electric Power University, Beijing, China
**China Electric Power Research Institute, Beijing, China
***Department of Electronics Engineering, Beijing Jiaotong University, Beijing, China
****Guangxi Electric Power Research Institute, Nanning, Guangxi Zhuang Autonomous Region, China

Abstract

Voltage and frequency stability issues occur in existing centralized power system due to the high penetration of renewable energy sources, which decrease grid absorptive capacity of them. The grid-connected inverter that mimics synchronous generator characteristics with inertia characteristic is beneficial to electric power system stability. This paper proposed a novel three-phase four-wire grid-connected inverter with an independent neutral line module that mimics synchronous generators. A mathematical model of the synchronous generator and operation principles of the synchronverter are introduced. The main circuit and control parameters design procedures are also provided in detail. A 10 kW prototype is built and tested for further verification. The primary frequency modulation and primary voltage regulation characteristics of the synchronous generator are emulated and automatically adjusted by the proposed circuit, which helps to supports the grid.

Key words: Distributed generator (DG), Grid-connected, Renewable energy source (RES), Synchronverter, Three-phase four- wire, Virtual synchronous generator (VSG)

I. INTRODUCTION

Environmental protection and sustainable energy issues have attracted a lot of attention from individuals, organizations and governments in recent years. Distributed Generators (DGs) using Renewable Energy Sources (RES) are one of the keys to address these challenges. RES such as photovoltaic and wind often need power electronic converters to serve as an interface between the source and the load or electric power system. In the past, the power grid was often assumed to have enough absorptive capacity for RES with randomness and volatility features. Today this assumption is sometimes untenable, especially with the high permeability of RES [1]. The main reason is that most grid-connected power electronics-based DGs are to be current sources with current control schemes, which try to inject as much active current into the grid as possible. These DGs seldom take consideration of the friendships between DGs themselves and electric power system until the grid code was released, where reactive power ability, leakage current elimination, and low voltage ride-through function are necessary.

However, frequency and voltage stability problems of the grid with a high penetration of RES are still unsolved because traditional centralized power system is built based on large voltage source synchronous generators. This is totally different from current source DGs in terms of behavior. Compared with synchronous generators, current source grid-connected inverters have a faster responses due to their inertia poverty, which help them "plug in and play". However, this also make it difficult for them to play with the grid interactively to maintain voltage and frequency stability at the same time.

Therefore, several voltage source grid-connected inverter theories and techniques have been proposed and developed in recent years. Droop control method and virtual synchronous

Manuscript received Jan. 13, 2016; accepted Jul. 14, 2016
Recommended for publication by Associate Editor Honnyong Cha.
†Corresponding Author: 12291159@bjtu.edu.cn
Tel: +86-18801271857, North China Electric Power University
*State Key Lab. of Alternate Electrical Power System with Renewable Energy Sources, North China Electric Power Univ., China
**China Electric Power Research Institute, China
***Dept. of Electronics Eng., Beijing Jiaotong University, China
****Guangxi Electric Power Research Institute, China

generator (VSG) theory are the main concern of academia and industry [2]-[7]. In addition, VSG with a controllable inertia has an inner ability to operate with the grid interactively. Several VSG concepts have been proposed and developed independently, named virtual synchronous generator, virtual synchronous machine, synchronverter and so on [2]-[8]. They mimic not only the steady-state characteristics of synchronous generators and transient features by applying swing equations to enhance the inertia [9]. The equivalence of virtual synchronous machines and frequency-droops for converter-based micro grids under certain conditions are demonstrated in [10]. Even an additional phase locked loop (PLL) technique is eliminated due to the inner self-synchronized feature of the VSG [11]. In addition to the active power consideration of grid-tie applications, VSG-based STATCOM for grids with a high penetration of renewable energy is evaluated and modeled in [12]. Virtual synchronous machine-based power control in active rectifiers for micro grids is developed and analyzed in detail in [13], and a single phase VSG application is discussed in [14].

Most of these analyses are presented based on a classic three-phase three-wire synchronous generator, while some power electronics-based inverters adopt the three-phase four-wire structure for three phase unbalance applications. Three-phase four-wire VSGs have not received a lot of attention in the literature. Therefore, the motivation behind this paper is to provide a three-phase four-wire VSG solution for single phase and three phase unbalance applications. Firstly, this paper describes the mathematical model of the synchronous generator and analyzes the working principle of the synchronverter. Secondly, a 10 kW prototype of the three-phase four-wire structure is introduced with a detailed design scheme for the main circuit and control parameters. Finally, detail experimental results from the prototype are provided for grid-friendly VSG verification.

II. Mathematical Model of a Synchronous Generator

The structure of an ideal synchronous generator model is shown in Fig. 1. For simplicity, it is assumed that there are no damping windings in the round rotor synchronous generator. In addition, the magnetic saturation effects and eddy currents are also neglected. Therefore, both the self-inductance of the stator windings and the mutual inductance between stator windings are constant. The self-inductance and mutual inductance are defined by L and $-M$ (M>0), separately. The three phase stator windings can be regarded as concentrated coils with the same structure, rotational symmetry and spatial displacement of 120 degrees.

According to Fig. 1, the mutual inductances between the field coil and each of the three stator coils is given by Equation (1):

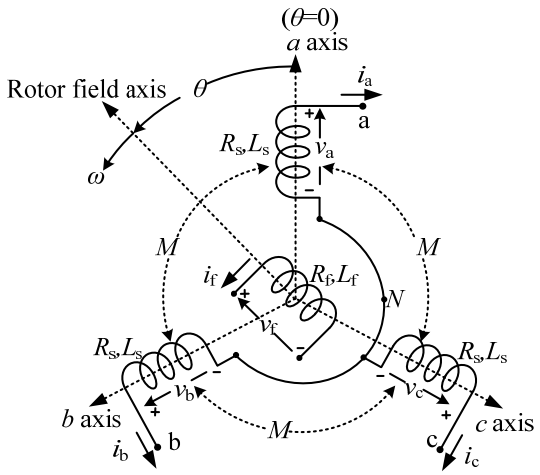

Fig. 1. Structure of an idealized three-phase round-rotor synchronous generator.

$$\begin{cases} M_{af} = M_f \cos\theta \\ M_{bf} = M_f \cos\left(\theta - \dfrac{2\pi}{3}\right) \\ M_{cf} = M_f \cos\left(\theta - \dfrac{4\pi}{3}\right) \end{cases} \tag{1}$$

where θ is the angle between the axis of the rotating magnetic field and the a-axis, M_f>0.

The mathematical model of the synchronous generator is shown in (2)-(7), where the excitation current i_f is constant.

$$v = -R_s i - \frac{\mathrm{d}\Phi}{\mathrm{d}t} = -R_s i - L_s \frac{\mathrm{d}i}{\mathrm{d}t} + e \tag{2}$$

$$e = M_f i_f \omega \widetilde{\sin\theta} \tag{3}$$

$$J\frac{\mathrm{d}\omega}{\mathrm{d}t} = T_M - T_e + D_p\omega \tag{4}$$

$$T_e = M_f i_f \left\langle i, \widetilde{\sin\theta} \right\rangle \tag{5}$$

$$Q = \left\langle i, e_q \right\rangle = -\omega M_f i_f \left\langle i, \widetilde{\cos\theta} \right\rangle \tag{6}$$

$$P = \left\langle i, e \right\rangle = \omega M_f i_f \left\langle i, \widetilde{\sin\theta} \right\rangle \tag{7}$$

Define:

$$\widetilde{\sin\theta} = \begin{bmatrix} \sin\theta \\ \sin\left(\theta - \dfrac{2\pi}{3}\right) \\ \sin\left(\theta + \dfrac{2\pi}{3}\right) \end{bmatrix}, \quad \widetilde{\cos\theta} = \begin{bmatrix} \cos\theta \\ \cos\left(\theta - \dfrac{2\pi}{3}\right) \\ \cos\left(\theta + \dfrac{2\pi}{3}\right) \end{bmatrix}$$

where T_e and T_m are the mechanical and electromagnetic torque, J and ω are the rotational inertia and angular speed of the rotor, $\boldsymbol{v}=[v_a,v_b,v_c]^T$ and $\boldsymbol{i}=[i_a,i_b,i_c]^T$ are the phase voltage and current of the stator, R_s is the resistance of the stator windings, $\boldsymbol{\Phi}=[\Phi_a,\Phi_b,\Phi_c]^T$ and $\boldsymbol{e}=[e_a,e_b,e_c]^T$ are the stator flux and EMF of each phase, D_p is the damping factor, and P and Q are the output active power and reactive power.

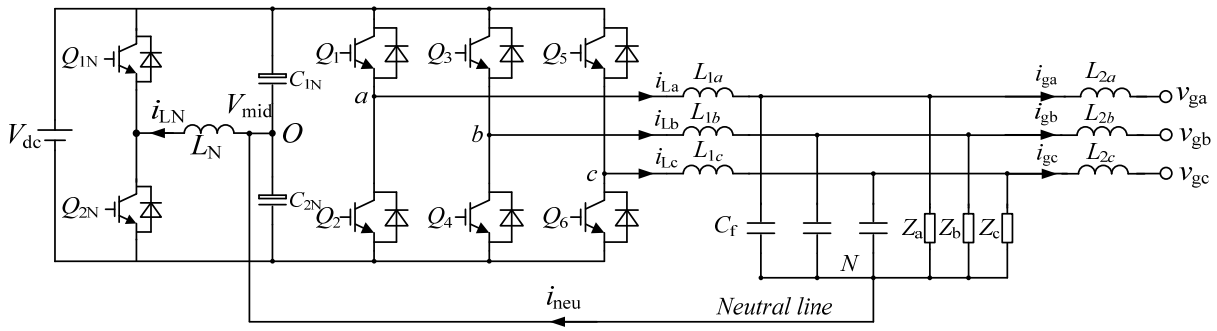

Fig. 2. Main circuit topology of a synchronverter.

According to the mathematical model of the synchronous generator, it can be found that the rotational inertia and the adjustable frequency and voltage characteristics of the synchronous generator play an active role in improving the stability of the power network. If the grid connected inverter of a distributed power system can simulate the rotating inertia and characteristics for the frequency modulation and voltage regulation of the synchronous generator in terms of the external characteristics, the stability of the distributed system and the absorptive capacity of the power grid can be improved.

III. OPERATION OF A SYNCHRONVERTER

Fig. 2 shows the main circuit topology of the proposed three-phase four-wire synchronverter that mimics the synchronous generator. It consists of a three phase six switch inverter and a unique voltage balancer, which provides the neutral line for single phase and unbalanced loads with a simple control approach.

The three phase six switch inverter adopts *LCL* output filters, where $L_{2a,b,c}$ are the line inductances for grid-connected applications. The induction electromotive force e of the synchronous generator, the stator impedance and the terminal voltage v are equivalent to the midpoint voltage of the bridge arm in Fig. 2, the impedance of inductance $L_{1a,b,c}$ and the voltage of capacitance C_f, respectively. This is the principle of the main circuit of the synchronverter emulating the synchronous generator.

A Digital Signal Processor (DSP) and its signal conditioning circuits constitute the control circuit of the synchronverter. The core control strategy, as shown in equations (3)-(6), is implemented with codes embedded in the DSP. According to equations (3)-(6), an open loop control block diagram without the frequency and voltage regulation can be obtained, as shown in Fig. 3. From Fig. 3, it can be seen that the inputs of the synchronverter control are the mechanical torque T_m and the product of the excitation current and the mutual inductance $M_f i_f$. The state variables are the current i of inductor L_1, the midpoint voltage of the bridge arm e, the virtual angular speed ω and the virtual electric angle θ. It can be seen from the upper part of

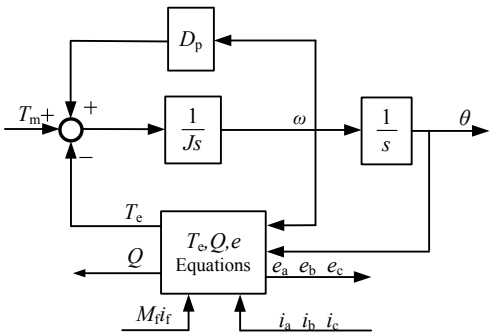

Fig. 3. Control block diagram of a synchronverter without control strategy.

Fig. 3 that equation (4) is realized by the relationship between ω, T_m ,and T_e in the control block diagram, which simulates the rotational inertia of the synchronous generator. It can also be seen that J is the virtual moment of inertia.

In order to improve the synchronverter control performance, closed loop controllers are added to provides the signals, T_m and $M_f i_f$. In addition, the active and reactive power are regulated, which helps the voltage and frequency stability of the system. The above objectives can be achieved by simulating the primary frequency modulation and the primary voltage regulation characteristic of the synchronous generator as shown in Fig. 4.

In the synchronverter control strategy, the active power control, also called frequency droop control in reference [7], is realized by primary frequency modulation. Compare the reference angular speed ω_r with the virtual angular speed ω, and then multiply the difference by a similar amount with the droop coefficient as a part of the mechanical torque T_m. According to equation (4), the frequency droop control is equivalent to the adjustment of the damping coefficient D_p when comparing the relationship between the mechanical torque T_m, the electromagnetic torque T_e and the angular speed ω. In Fig. 4, D_p is the sum of the frequency droop coefficient and the damping coefficient. That is:

$$D_p = -\frac{\Delta T}{\Delta \omega} \tag{8}$$

where the change of the virtual electromagnetic torque and the change of the angular speed are defined as ΔT and $\Delta \omega$,

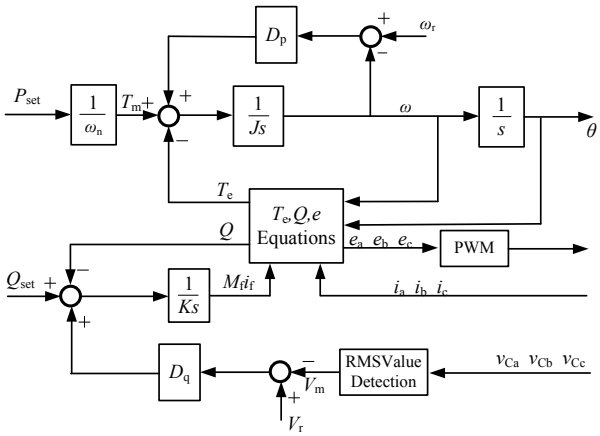

Fig. 4. Control block diagram of a synchronverter with real and reactive power regulation.

separately. In addition, the mechanical torque T_m can be obtained from the ratio of the reference active power P_{set} and the nominal angular speed ω_n.

Similarly, the control of the reactive power Q is realized by primary voltage regulation, which is also called voltage droop control. The voltage droop coefficient is defined as D_q. ΔU can be obtained from the difference between the power grid voltage amplitude U_m and the reference voltage U_r. The required reactive power conversion is $-\Delta Q$. Thus, the following is obtained:

$$D_q = -\frac{\Delta Q}{\Delta U} \tag{9}$$

Therefore, the product of ΔU and the voltage droop coefficient D_q can be obtained. Then add them to the difference between the reactive power Q (calculated by equation (6)) and the reference value Q_{set}. The resulting signal is then fed to an integrator with a gain of $1/K$ to generate $M_f i_f$.

To conclude, a control block diagram of the synchronverter with regulation of the real and reactive power is shown in Fig.4. The phase angle θ of the three-phase reference voltages e_a,e_b,e_c can be obtained by the active power loop, and the amplitude $M_f i_f \omega_n$ can be obtained by the reactive power loop. Then, the reference voltage can be calculated according to equation (3) (Since the angular frequency has little effect on the amplitude of the voltage, the nominal angular frequency ω_n takes the place of ω). The triangular wave, used as carrier wave, intersects with the three-phase reference voltage modulation wave. This results in the three phase sinusoidal pulse width modulation wave to drive switch tubes on each bridge arm.

Since the synchronverter emulates the rotating inertia and the excitation regulation performance of the synchronous generator, the two have the same static stable operation principle when both are connected to the grid. In other words, when the angle δ (power angle) between the capacitor voltage of the synchronverter and the grid voltage is less than $\pi/2$, it meets the static stable operation conditions.

TABLE I
PARAMETERS OF SYNCHRONVERTER

Parameters	Values	Parameters	Values
DC voltage U_{dc}/ V	800	Switching frequency f_s/	10 kHz
Grid phase voltage U_g/ V	220	Inductor L_1/ mH	1.6
Grid frequency f_g/ Hz	50	Capacitor C_f/μF	10
Rated power P/ kW	10	Inductor L_2/μH	500
		Capacitor C_N/μF	1000

IV. DESIGN OF THE MAIN CIRCUIT AND CONTROL PARAMETERS

A. Main Circuit Design

The main circuit of the synchronverter and the traditional inverter are quite similar to each other. Several basic constraints are as given as follows: the reactive power of the filter capacitor is designed to account for about 5% of the rated output power ($C_f \le 5\%P_o/(3\cdot 2\pi f_o \cdot V_g^2) = 10.9\mu F$); the current ripple of inductance L_1 is designed to be less than 40% of the current peak at full load so as to reduce the iron loss of magnetic components; the harmonic current amplitude of the multiple times of the switching frequency is less than 0.3% of the amplitude of the fundamental wave current. According to the above constraints, *LCL* filter parameters and other electrical parameters are shown in Table I.

In the main circuit of the three phase inverter shown in Fig. 2, the maximum voltage stress of the active switch is the bus voltage V_{dc}=800V. This was chosen mainly based on the tolerance of the voltage and current stress. Considering the impact of the circuit parameters, the maximum voltage of the switching device is higher than that of the bus voltage. For the engineering designs, a 1.5 times safety margin is generally chosen. Therefore, switches with a 1200V rated voltage were selected. From the current point of view, the mean current flowing through the filter inductor is I_{Lrms}=22.7 A. This also flows through the switches, with a maximum peak current 35.2 A. Thus, switches with a rated current greater than 52.8A considering a 1.5 times safety margin were selected. In this paper, the IGBT module CM100DY-24NF from Mitsubishi Corporation was chosen. Its rated voltage and current are U_{CES}=1200 V and I_{C25}=100 A , respectively.

B. Control Parameter Design

Grid codes allow line frequency changes between 49Hz~51Hz. They also allow the voltage amplitude to vary between the 90%~110% of rated voltage amplitude. Therefore, the design principles of D_p and D_q are set as follows: the output active power of the inverter increases 100% (10kW) when the grid frequency drops 1 Hz. In addition, the output reactive power increases 100% (10kVar) when the grid voltage magnitude drops 10%.

According to equation (8), the following is obtained:

$$D_p = -\frac{\Delta T}{\Delta \omega} = \frac{\Delta P}{\omega \Delta \omega} = \frac{10\,000}{2 \times 50\pi \times 2\pi} \approx 5$$

Select a frequency droop control time constant of τ_f=0.01s, and then the moment of inertia becomes:

$$J = D_p \tau_f = 5 \times 0.01 = 0.05$$

According to equation (9), the following is obtained:

$$D_q = -\frac{\Delta Q}{\Delta v} = \frac{10\,000}{220 \times \sqrt{2} \times 10\%} \approx 321$$

Select a voltage droop control time constant of τ_v=0.36 s, then:

$$K \approx \omega_n D_q \tau_v = 100\pi \times 321 \times 0.36 \approx 36303$$

Last but not least, it is found that the moment of inertia and the damping coefficient can be set artificially, which provide additional control freedom compared with existing synchronous generators [15]-[16].

C. Independent Neutral Line Module Design

The capacitor C_N plays an important role in the operation of the neutral voltage control. It is a compromise between the value of C_N and the control difficultly for the neutral point voltage control. Traditionally, there are two approaches. The simplest way is a split DC link. However, it needs many serial-parallel capacitors since unbalanced current flows through the capacitors. The other method is to use an additional fourth branch without split capacitors. However, the additional fourth leg must be controlled with the other three legs because the four legs are coupled together. It is quite complicated from a control view point. The way it is used here is a combination of the two methods above, where the control of the middle point is decoupled from the three phase three leg inverter.

Assume that the voltages across the capacitors C_{1N} and C_{2N} (C_{1N}=C_{2N}=C_N) are defined as are V_{C1N} and V_{C2N}, respectively.

As a result, the shift voltage of the middle point is:

$$\begin{aligned} V_{shift} &= V_{C1N} - V_{C2N} \\ V_{dc} &= V_{C1N} + V_{C2N} \end{aligned} \tag{10}$$

According to the Kirchhoff's current law:

$$\begin{aligned} i_{LN} &= i_{neu} + i_c \\ i_c &= -i_{c1} - i_{c2} = \\ &-C_N \frac{d(V_{dc}/2 - V_{shift})}{dt} - C_N \frac{d(-V_{dc}/2 - V_{shift})}{dt} \\ &= 2C_N \frac{dV_{shift}}{dt} \end{aligned} \tag{11}$$

Then:

$$V_{shift} = \frac{1}{2C_N} \int_0^t (i_{LN} - i_{neu}) dt \tag{12}$$

Equation (12) means that the capacitors here are not necessarily very large like those in the split DC link approach if the neutral current is controlled to flows through the inductor rather than the middle point capacitors. In addition, this can be achieved by the impedance matching method where the impedance of the inductor branch should be far less than that of the capacitor branch with the current mode control approach introduced.

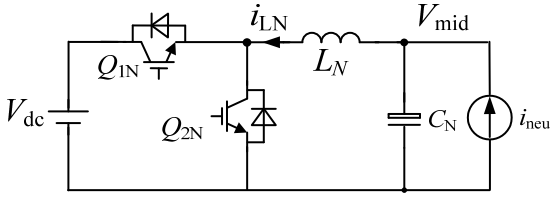

(a) Equivalent circuit.

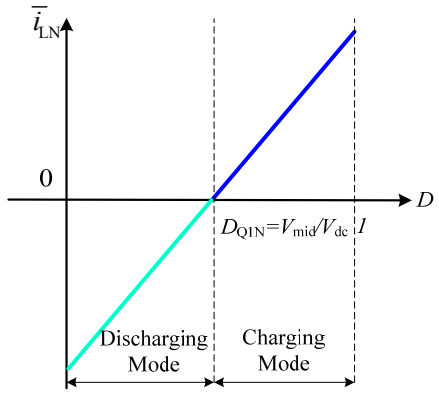

(b) Relationship between Q_{1N} , Q_{2N} gate signals and inductor current i_{LN}.

Fig. 5. Equivalent circuit of independent neutral line module.

At the same time, it is necessary for the current loop to make sure the neutral line current i_{neu} is well tracked. Considering that low frequency current during unbalanced loads, rather than the switching ripple current, is the main concern of this topic, a current loop designed with the traditional crossover frequency and phase margin method is fast enough to track the low frequency neutral line current [17], where the independent neutral line module behaves like an ideal current source. Therefore, the detail current loop design procedures are ignored due to limited pages.

In the neutral line module, the current i_{neu} caused by the imbalance can be viewed as a current sink. The module is a Buck/Boost bidirectional converter or a synchronous Buck converter from a topology point of view [17]. The hardware equivalent circuit and control block diagram are shown in Fig.5 and Fig. 6, respectively.

Therefore, a control block diagram of the independent neutral line module with double control loops is illustrated as shown in Fig. 6. In addition, it is found that the additional leg is decoupled controlled without considering the operation modes of the other three legs.

A unified control method is adopted with the gate signal in a complementary way, and Q_{1N} is the only main controlled switch rather than both the Buck and Boost controllers. The Buck/Boost bidirectional converter can be a Buck or Boost converter depending on the duty ratio changes as illustrated in Fig. 5(b) [17].

Ideally, the duty ratio of Q_{1N} should be D_{Q1N}=V_{mid}/V_{dc}=0.5 if

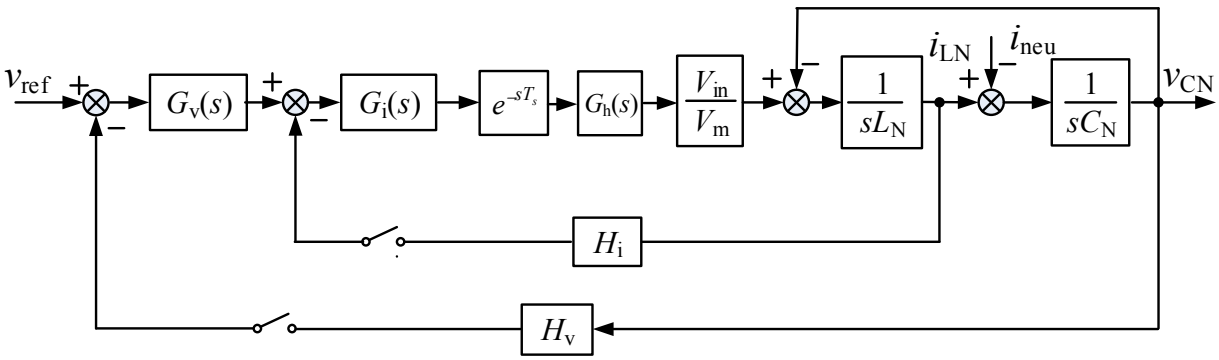

Fig. 6. Control block diagram of independent neutral line module.

the shift voltage of the middle point is zero. If D_{Q1N}>0.5, the independent neutral line module is a Buck converter in the charging mode, which lifts the V_{mid} voltage across the lower capacitor C_{2N}. If D_{Q1N}<0.5, the energy stored in the lower capacitor C_{2N} is transferred to the high voltage bus, which decreases V_{mid}. Therefore, the voltage balance of the split bus is achieved.

$G_v(s)$ in Fig. 6 is a voltage outer loop regulator designed as a double pole double zero adjuster. This expression can be written as:

$$G_v(s)=\frac{K(1+T_{z1}s)(1+T_{z2}s)}{s(1+T_{p1}s)} \tag{13}$$

$G_i(s)$ in Fig. 6 is a current inner loop regulator designed as a proportional regulator with gain of 1. e^{-sTs} is the one-beat delay introduced by the digital control. In addition, $G_h(s)$ is the transfer function of the zero-order holder and the expression can be written as:

$$G_h(s)=\frac{1e^{-sT_s}}{s} \tag{14}$$

In Fig. 6, V_{in} is the input voltage on the DC side; V_m is the amplitude of the triangular carrier; H_v is the midpoint voltage feedback coefficient; and H_i is the neutral line inductor current feedback coefficient, which feeds back inductor current so as to achieve active damping.

From the view point of impedance analysis, the Buck/Boost bidirectional converter or synchronous Buck converter in Fig. 5 is simplified as an impedance model and the simplified equivalent circuit is shown in Fig. 7. Z_C is the closed loop output impedance of the capacitor branch, whose expression is the capacitive reactance of capacitor $1/sC_N$. Z_L is the closed loop output impedance of the inductor branch, whose expression is [18]:

$$Z_L(s)=\frac{sL_N+r_{vir}}{1+\frac{V_{in}}{V_m}G_v(s)} \tag{15}$$

where r_{vir} is the virtual resistance that the neutral line inductance current feeds back to the inductance branch. The expression is:

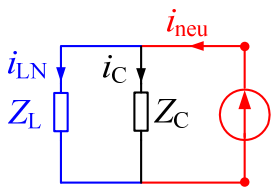

Fig. 7. Equivalent circuit of independent neutral line module based on impedance model.

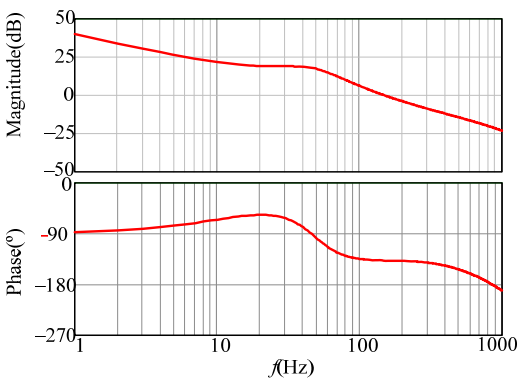

Fig. 8. Bode plot of the system loop gain.

$$r_{vir}=\frac{V_{in}}{V_m}H_i e^{-1.5sT_s} \tag{16}$$

In Fig. 6, in order to achieve the control of the middle bus voltage, it is necessary to control the neutral line current to go through the inductor branch and to minimize the closed loop impedance of the inductor branch at 50 Hz as far as possible. In other words, it is only possible increase the gain of the voltage regulator G_v(s) at 50 Hz. Therefore, in the design of the closed loop control parameters of the independent line module, it is necessary to ensure the system stability and to increase the gain of G_v(s) at 50 Hz as far as possible.

The following is the final design parameters. In the voltage outer loop regulator $G_v(s)$, the gain is K=7.91, the zero point is T_{z1}=0.0106, the pole is T_{p1}=0.000106, and the neutral line inductor current feedback coefficient is H_i=0.01. Fig. 8 shows bode plots of the system loop gain after compensation. From Fig. 8, it can be seen that the system cut off frequency is f_c=150 Hz, the phase margin is PM=42°, and the system is stable.

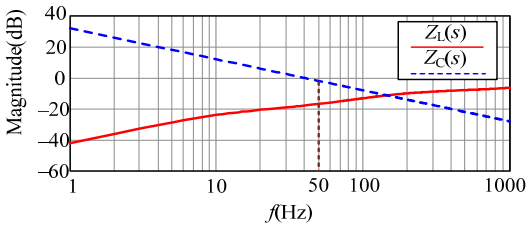

Fig. 9. Amplitude-frequency curve of output impedance in the inductor and capacitor branch.

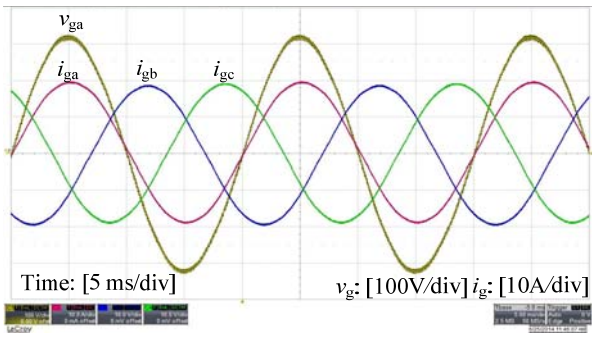

Fig. 10. Steady-state experimental waveforms when P_{set}=10 kW, Q_{set}=0 Var.

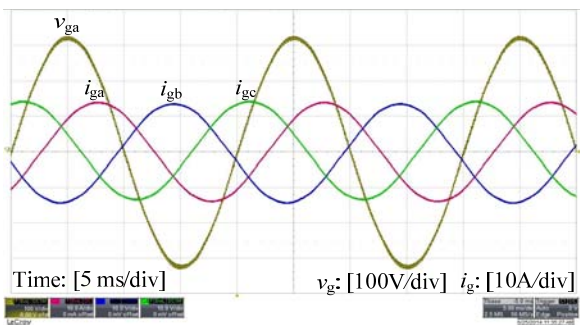

(a) Steady-state experimental waveforms when Pset =5 kW, Qset =5 kVar(inductive).

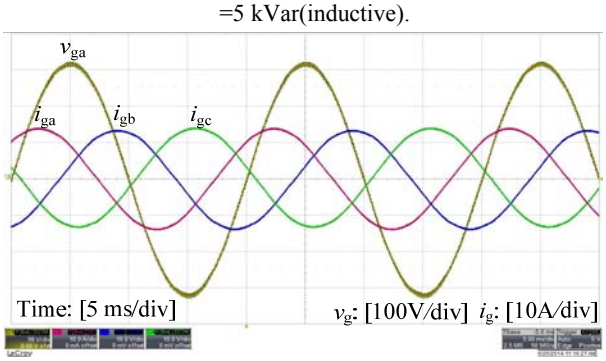

(b) Steady-state experimental waveforms when Pset =5 kW, Qset =5 kVar(capacitive).

Fig. 11. Steady-state experimental waveforms when P_{set} =5 kW, Q_{set} =5 kVar.

At the same time, in order to ensure that the neutral current is flowing through the inductor branch, it is necessary to ensure that the closed loop impedance of the inductor branch is far less than that of the capacitor branch at 50 Hz. Fig. 9 shows the amplitude-frequency curve of the output impedance in the

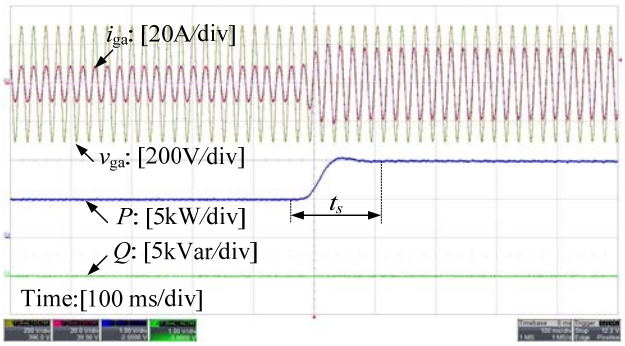

(a) Active power increases 5kW when grid frequency drops 0.5Hz.

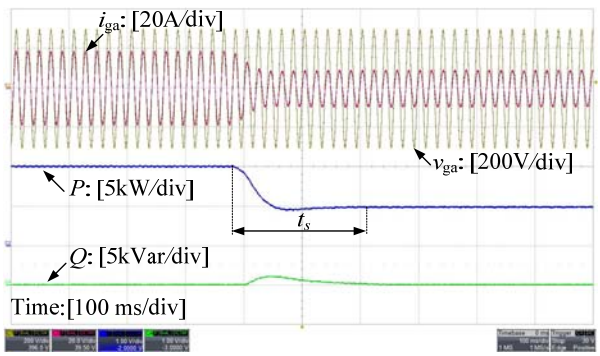

(b) Active power decreases 5kW when grid frequency rises 0.5Hz.

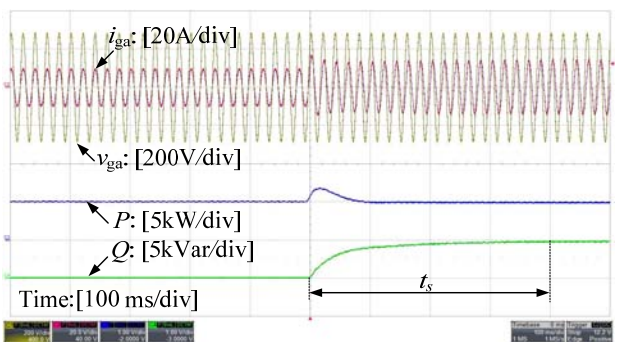

(c) Reactive power increases 5kVar with grid magnitude drops 0.5%.

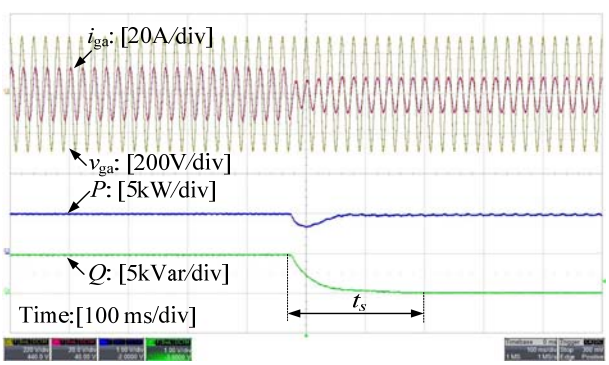

(d) Reactive power increases 5kVar with grid magnitude rises 0.5%.

Fig. 12. Dynamic performance with grid magnitude and frequency changes.

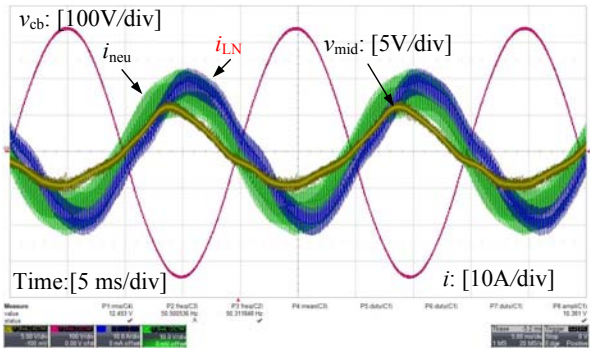

Fig. 13. Neutral line current with 100% unbalanced load.

inductor and capacitor branch. In Fig. 9, the closed loop output impedance of the inductor branch X_L is 0.14 Ω at 50 Hz, and the closed loop output impedance of the capacitor branch X_C is 0.80 Ω. The closed loop output impedance of the capacitor branch is far greater than that of the inductor branch. As a result, the closed loop parameters design meets the requirements.

V. Experimental Verification

In order to verify the proposed topology and its control schemes, a 10 kW prototype was built and tested in the laboratory. The detail parameters are listed in Table I in section IV. The ac grid is simulated by a programmable AC power supply (Chroma 61512).

Fig. 10 and Fig. 11 show steady-state experimental waveforms under different conditions. In Fig. 10, the power command of the synchronverter prototype was set as P_{set}=10 kW and Q_{set}=0 Var, and it shows that the phase *a* capacitor voltage and its corresponding grid current have the same frequency and phase angle. When the active power and reactive power are set as 5 kW and 5 kVar in Fig. 11, the phase *a* capacitor voltage and its corresponding grid current have the same frequency but different phase angles, since they are determined by the capacitive or inductive reactive power order.

Fig. 12 shows the dynamic interactive process between the synchronverter and the grid. It is found that the active power increases from 5kW to 10kW when the grid frequency drops by 0.5Hz, and vice versa. When the voltage amplitude decreases by 5%, the synchronverter provides an extra 5kVar of reactive power to support the grid. The primary frequency modulation and primary voltage regulation characteristic of the synchronverter are both clearly illustrated.

Besides that, when the synchronverter works with three unbalanced load, it operates well due to the proposed independent neutral line module. Fig. 13 illustrates the related waveforms with a 100% unbalanced load (a-phase 3 kW, b-phase no-load, c-phase 3 kW). As can be seen from Fig. 13, the neutral line current i_{neu} is about 16 A rms, which is the main contribution to the inductor current i_{LN}. Therefore, little current flows into the capacitor bank and the fluctuation of the midpoint voltage is quite small with about a ±5 V variation. It shows that the voltage across the DC side is stable and that the proposed control strategy operates well.

VI. Conclusions

Based on the idea of operating an inverter as a synchronous generator, this paper proposes a novel three-phase four-wire grid-connected synchronverter, which operates with the grid interactively. The mathematical model, operation principles, neutral line module, key components and control schemes are provided in detail. A 10kW prototype is built and tested, which verifies the novel three-phase four-wire grid-connected synchronverter features:

1) The primary frequency modulation and primary voltage regulation characteristics of the synchronous generator are emulated and automatically adjusted by the proposed synchronverter, which helps the synchronverter support the grid. The communication line and supervisory control unit are no longer necessary, which helps the autonomous power system with more power electronics converters.

2) The independent neutral line module provides the neutral line for single phase and unbalanced loads with an independent control approach. The control schemes of the neutral line module and the three phase six switch inverter are totally decoupled, which simplifies the synchronverter control approach.

Acknowledgment

The research was carried out in the frame of the 2016 national key R & D program to support National Natural Science Foundation of China(51507158), Science and Technology Project of SGCC(PD71-16-024&PD71-16-023) and Low-carbon Winter Olympics of Integrated Smart Grid Demonstration Project (2016YFB0900501).

References

[1] E. Ghiani and P. Fabrizio, "Smart inverter operation in distribution networks with high penetration of photovoltaic systems," *Journal of Modern Power Systems and Clean Energy*, Vol. 3, No. 4, pp. 504-511, Dec. 2015.

[2] J. C. Vasquez, J. M. Guerrero, A. Luna, P. Rodriguez, and R. Teodorescu, "Adaptive droop control applied to voltage-source inverters operating in grid-connected and islanded modes," *IEEE Trans. Power Electron.*, Vol. 56, No. 10, pp. 4088-4096, Oct. 2009.

[3] M. R. Miveh, M. F. Rahmat, A. A. Ghadimi, and M. W. Mustafa, "Power quality improvement in autonomous microgrids using multi-functional voltage source inverters: a comprehensive review," *Journal of Power Electronics*, Vol. 15, No. 4, pp. 1054-1065, Jul. 2015.

[4] Q. Zhang, Y. Liu, C. Wang, and N. Wang, "Parallel operation of microgrid inverters based on adaptive sliding-mode and wireless load-sharing controls," *Journal*

of Power Electronics, Vol. 15, No. 3, pp. 741-752, May 2015.

[5] H. P. Beck and R. Hesse, "Virtual synchronous machine," in *9th International Conference on Electrical Power Quality and Utilisation (EPQU)*, pp. 1-6, 2007.

[6] J. Driesen and K. Visscher, "Virtual synchronous generators," in *IEEE Power and Energy Society General Meeting - Conversion and Delivery of Electrical Energy in the 21st Century*, pp. 1-3, 2008.

[7] Q.-C. Zhong and G. Weiss, "Synchronverters: inverters that mimic synchronous generators," *IEEE Trans. Ind. Electron.*, Vol. 58, No. 4, pp. 1259-1267, Apr. 2011.

[8] P. Rodriguez, I. Candela, and A. Luna, "Control of PV generation systems using the synchronous power controller," in *IEEE Energy Conversion Congress and Exposition (ECCE)*, pp. 993-998, Sep. 2013.

[9] Z. Lv, Y. Liang, and Z. Zheng, "Virtual synchronous generator and its applications in micro-grid," *Proceedings of the CSEE,* Vol. 34, No. 16, pp. 591-2603, 2014.

[10] S. D'Arco and J. A. Suul, "Equivalence of virtual synchronous machines and frequency-droops for converter-based micro grids," *IEEE Trans. Smart Grid*, Vol. 5, No. 1, pp. 394-395, Jan. 2014.

[11] Q.-C. Zhong, P.-L. Nguyen, Z. Ma, and W. Sheng, "Self-synchronized synchronverters: Inverters without a dedicated synchronization unit," *IEEE Trans. Power Electron.*, Vol. 29, No. 2, pp. 617–630, Feb. 2014.

[12] C. Li, R. Burgos, I. Cvetkovic, D. Boroyevich, L. Mili, and P. Rodriguez, "Analysis and design of virtual synchronous machine based STATCOM controller," in *IEEE 15th Workshop on Control and Modeling for Power Electronics (COMPEL)*, pp. 1-6, 2014.

[13] A. Perera, "Virtual synchronous machine-based power control in active rectifiers for micro grids," *MSc. Thesis*, *Norwegian University of Science and Technology*, Trondheim, Norway, 2012.

[14] Y. Hirase, K. Abe, K. Sugimoto, and Y. Shindo, "A grid-connected inverter with virtual synchronous generator models of algebraic type," *IEEJ Trans. Power Energy*, Vol. 132, No. 4, pp. 371-380, 2012.

[15] J. Alipoor, Y. Miura, and T. Ise, "Power system stabilization using virtual synchronous generator with alternating moment of inertia," *IEEE J. Emerg. Sel. Topics Power Electron.*, Vol. 3, No. 2, pp. 451-458, Jun. 2015.

[16] J. Alipoor, Y. Miura, and T. Ise, "Distributed generation grid integration using virtual synchronous generator with adoptive virtual inertia," in *IEEE Energy Convers. Congress and Exposition (ECCE)*, pp. 4546-4552, 2013.

[17] J. Wang, F. Zhang, C. Gong, and R. Chen, "Modeling and analysis of a Buck/Boost bidirectional converter with developed PWM Switch model," in *IEEE 8th International Conference on Power Electronics and ECCE Asia (ICPE & ECCE),* pp. 705-711, 2011.

[18] L. Zhang, X. Ren, and X. Ruan, "A band-pass filter incorporated into the inductor current feedback path for improving dynamic performance of the front-end dc-dc converter in two-stage inverter," *IEEE Trans. Ind. Electron.*, Vol. 61, No. 5, pp. 2316-2325*,* May 2014.

Qian Tan was born in Wangcheng, Hunan Province, China, in 1983. He received his B.S. degree in Electrical Engineering from China Agricultural University, Beijing, China, in 2005; his M.S. degree in Electrical Engineering from Tsinghua University, Beijing, China, in 2009; and his Ph.D. degree in Intelligent Distribution Networks and Distributed Generation from the North China Electric Power University, Beijing, China, in 2013. From 2005 to 2009, he was engaged in substation running and scheduling managements for the Beijing Electric Power Company, Beijing, China. His current research interests include distribution automation and intelligent distribution network. In 2013, he was awarded first place for State Grid Corporation of Science and Technology Progress Prize Award.

Zhipeng LV was born in Binzhou, Shandong Province, China. He received his B.S., M.S., and Ph.D. degrees from Hunan University, Changsha, China, in 2007, 2010, and 2012, respectively. He joined the Power Distribution Department of the China Electric Power Research Institute, Haidian District, Beijing, China, in 2012. From 2012 to 2013, he was an Engineer in the Micro-grid Research Section, where he worked on the development of micro-grid coordination control and power inverters for renewable energy integration. He was named a Senior Engineer, in 2013. His current research interests include power electronics and control, virtual synchronous machines, power electronic power systems, power inverter adaptive control, and the fault diagnosis of electronic devices.

Bei Xu was born in Qingdao, Shandong Province, China, in 1994. She received her B.S. degree in Electronics Engineering from Beijing Jiaotong University, Beijing, China, in 2016, where she is presently working towards her M.S. degree. Her current research interests include power electronics and control, microgrid power systems, and the application of power electronics in renewable energy systems and electrified railway systems.

Wenqian Jiang was born in Yongzhou, Hunan Province, China. She received her B.S. and M.S. degrees from Hunan University, Changsha, China, in 2007 and 2010, respectively. From 2010 to 2016, she worked at the Guangxi Electric Power Research Institute, Nanning, China. From 2010 to 2012, she was an Junior Engineer of the Metering Center and was named an Engineer, in 2012. She has taken charge of more than ten projects of the China Southern Power Grid and has received more than thirty awards due to her outstanding contributions. From 2010 to 2016, she worked at the Guangxi Electric Power Research Institute, Nanning, China. Her current research interests include measuring instruments, wind turbines and photovoltaic detection.

Xin Ai received his B.S. degree from the Nanjing Institute of Technology (now Southeast University), Nanjing, China, in 1985; his M.S. degree from the China Electric Power Research Institute, Beijing, China in 1988; and his Ph.D. degree from the North China Electric Power University (NCEPU), Beijing, China, in 1999, all in Electrical Engineering. He was a Senior Research Scholar with Brunel University, London, UK, in 2003. He was the Director of the Institute of Power Systems, NCEPU, where he was engaged in research and teaching on the power system and automation. He is presently working as a Professor and a Doctoral Tutor with the School of Electrical and Electronic Engineering, NCEPU. His current research interests include power system analysis and control, new energy and micro-grid power systems.

Qingchang Zhong (M'04–SM'04) received his Ph.D. degree in Control and Engineering from Shanghai Jiao Tong University, Shanghai, China, in 2000; and his Ph.D. degree in Control Theory and Power Engineering from Imperial College London, London, UK, in 2004. He is the Chair Professor of Control and Systems Engineering in the Department of Automatic Control and Systems Engineering, University of Sheffield, Sheffield, UK, and a Specialist recognized by the State Grid Corporation of China. He is a Distinguished Lecturer of the IEEE Power Electronics Society and the UK Representative to the European Control Association. He coauthored four research monographs: *Control of Power Inverters in Renewable Energy and Smart Grid Integration* (New York, NY, USA: Wiley-IEEE Press, 2013), *Robust Control of Time-Delay Systems* (New York, NY, USA: Springer-Verlag, 2006), *Control of Integral Processes with Dead Time* (New York, NY, USA: Springer-Verlag, 2010), and, *Completely Autonomous Power Systems (CAPS): Next Generation Smart Grids*, which is scheduled for publication by Wiley-IEEE Press, in 2016. He proposed the architecture for next-generation smartgrids based on the synchronization mechanism of synchronous machines to achieve autonomous operation for power systems. His current research interests include power electronics, advanced control theory and the integration of both, together with applications in renewable energy, smart grid integration, electric drives, electric vehicles, aircraft power systems, and high-speed trains.